Journal of Engg. Research Vol. 7 No. (2) June 2019 pp. 125-142

Infrared thermography and finite element method applied to the detection of internal defects in reinforced concrete slabs

Abdelhamid Noufid* and Sougrati Belattar

Department of Physics, Faculty of Science Semlalia, Moulay Abdellah Street, Marrakech, 40000, Morocco
**Corresponding Author: abdelhamid.noufid@ced.uca.ac.ma*

ABSTRACT

The development of numerical methods has made digital simulation a very important tool in the field of industry and in various fields of scientific research. In this work, we seek to make a study as complete as possible on the behavior of the slabs of structures, according to the internal anomalies, which can touch these elements, due to, on one hand, the effect of aging and the seism and, on the other hand, the permanent climate changes to which these elements are subjected or simply to accidents such as explosion. This article deals with the application of infrared thermography in the detection of anomalies in a reinforced concrete slab. This defect takes several forms, namely, horizontal, vertical, oblique, or spherical. In this one, we will study the defect in inclined and spherical position while varying on one hand the properties of the slab and, on the other hand, the characteristics of the defect. With finite element simulation software, different simulations have been carried out to derive results on infrared thermography in reinforced concrete slabs, according to this study, the detection of these cracks by infrared if and only if a number of conditions are available. However, this method is impotent in some cases, which necessitates deviating from the limits of its use, which we will address in this work.

Keywords: Reinforced concrete; Thermal image; Simulation; Defect; Detection.

INTRODUCTION

Non-Destructive Testing (NDT) of materials and structures is part of the general framework of quality improvement, safety, and concerns a wide range of fields. Infrared thermography (IRT) is part of non-destructive testing (NDT), used to detect voids, delamination, and other anomalies in concrete and detect water entry points in buildings (IAEA, 2002 & ELAFI et al., 2017). It is based on infrared radiation (below red), a form of electromagnetic radiation with longer wavelengths than those of visible light (Usamentiaga et al., 2014); thus, infrared measuring devices are required to acquire and process this information (Vollmer et al., 2011). It is the infrared camera which makes it possible to observe this type of rays in the absence of light; it provides two-dimensional thermal images that allow a comparison between the zones of the target. These thermal images make it possible to give a clear idea of the presence of a defect by measuring the temperature field of an external surface of an object. Indeed, the presence of an anomaly creates an observable thermal disturbance on the corresponding thermal image, such as water infiltration and moisture (Bomberg et al., 1988 & Ljungberg, 1994). A wet mass in a wall has a differentiated thermal inertia that can be discovered using IRT. Recent applications of IRT for moisture detection can be found in Maierhofer et al. (2009) & Grinzato et al. (2002), which use IRT for sub-surface moisture detection in masonry structures and for moisture mapping in ancient buildings, respectively. Moisture detection using IRT is not limited to buildings. It can also be applied to soil (Sugiura et al., 2007) or aircraft structures (Vavilov et al., 2004). The presence of water inside aircraft structures may lead to ice formation with a volume variation and consequent mechanical stresses. In addition, among the applications of

thermography in the building, one can quote the detection of a delamination in the structures in concrete or reinforced concrete (Al-Kassir et al., 2005). This gives the manager a quick reaction time to intervene in terms of readjustment or rectification on the operating parameters of the structure or on its use, to repair in order to minimize or stop deterioration of the structure and to prevent against any accident. As part of the diagnostic policy for structures, it is necessary to know and study the capabilities of infrared thermography to detect defects in concrete (Kathleen et al., 2004), especially internal cracks in solid reinforced concrete slabs. Internal cracks may be present within the slab and not be detected with conventional control means (Belattar et al., 2012). Active IRT is mostly used in non-destructive testing applications, where an external stimulus is applied to the specimen in order to induce relevant thermal contrasts between regions of interest (Ibarra et al., 2003).

DESCRIPTION OF THE GENERAL PROBLEM

In winter, the water contained in the cracks at the level of a reinforced concrete slab freezes, its volume increases, and exerts a force, which tends to propagate the crack (Fig. 1). Ice also plays the role of glue that makes the concrete on both sides of the crack remains attached. When spring arrives, the ice in the crack melts, and the concrete of the lower part comes off and falls.

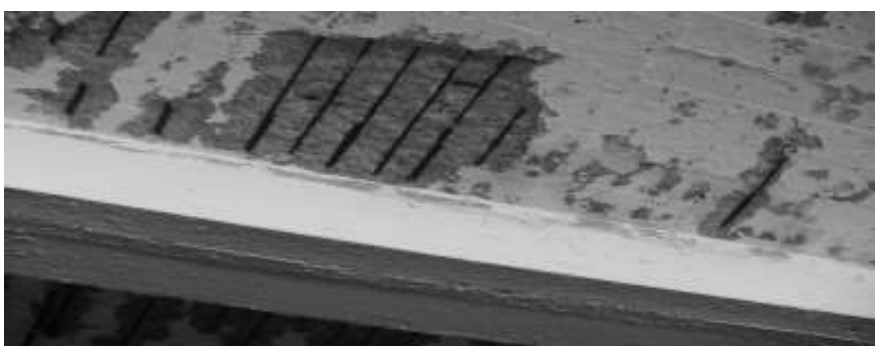

Fig. 1. Concrete blocks stand out from a bridge.

Internal cracks may be present within the slab and not be detected with conventional control means. Thereafter comes this research, which aims to study the ability of infrared thermography to detect the presence of ice in cracks during this season. The illustration of this phenomenon can be schematized in Fig. 2.

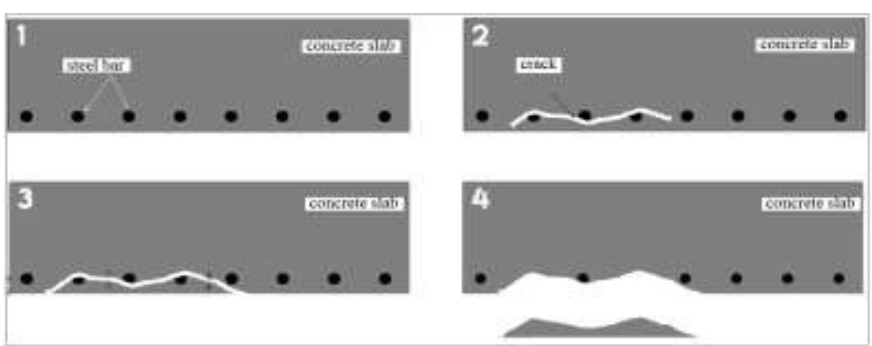

Fig. 2. Schematization of the problem.

PRESENTATION OF THE MODEL

The tests were carried out on a concrete slab 1 m long, 1 m wide, and 20 cm thick (Fig. 3).

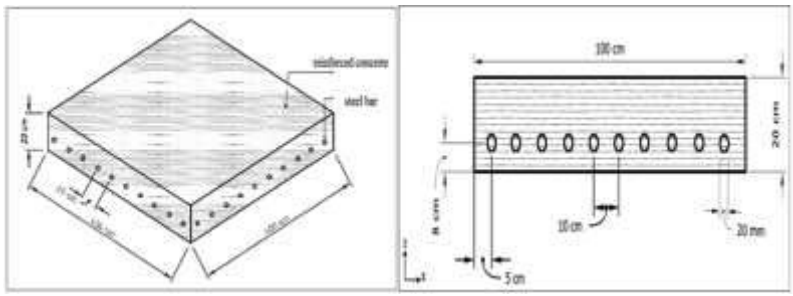

Fig. 3. Geometry of the slab.

This slab contains two rows of reinforcement located at a depth p = 8 cm from the lower surface of the slab. The steel bars are spaced at a distance d = 10 cm from each other.

SIMULATIONS

In order to illustrate the considerations mentioned above, we present the results of calculations of the thermal response of the reinforced concrete slab located at the following thermal conditions:

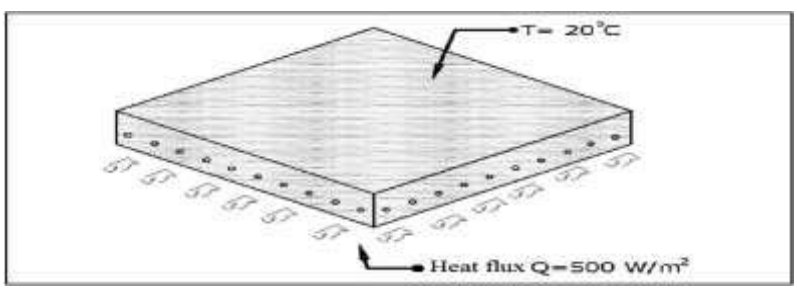

Fig. 4. Boundary conditions of the slab.

The bottom surface of the structure is uniformly heated with a permanent heat source, the power of the heat flux transmitted by this source is 500 W/m^2, the upper face being maintained at a constant temperature T = 20°C, and the other faces are supposed to be isolated (Q=0 W/m^2). The initial temperatures considered for the lower surface and for the ambient environment were 20°C (Fig.4). The materials used in this study are characterized by the thermophysical properties grouped in the table 1.

Table 1. Thermophysical properties of materials used.

Material	Thermal Conductivity (W/m.K)	Density (Kg/m^3)	Heat capacity (J/Kg.K)
Concrete	1.8	2300	880
Structure steel	44.5	7850	475
Ice	1.05	918	2052

Study of oblique cracks

The appearance of an oblique crack in a concrete slab is the result of several factors. These factors are caused by

- Differential settlement (Laure, 2006), linked to a clay soil. The clays swell in durably rainy weather, and shrink during acute or prolonged drought episodes;
- An accidental event, such as pipe breakage (Nguyen et al., 2005).

However, some factors are more prevalent such as the poor quality of concrete used in construction. External causes may also cause such cracks. In this study, we chose a system of the same dimensions as the previous one in which an oblique crack is introduced (Fig. 5), of length L = 4 cm and of height h = 10 cm, to incline of an angle of 45 degree. The power of the heat flux transmitted by the source is 500 W/m^2.

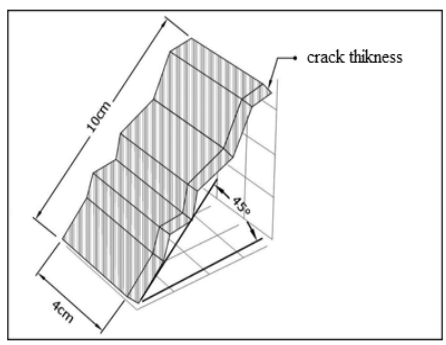

Fig. 5. Geometry of the oblique crack.

The thermographic images given below represent the results of the simulations of the lower surface of the slab, and the curves represent the temperature difference along the lines studied. In this section we will make a parametric and geometric study for the oblique cracks in order to know the influence of the thickness and the position on the detectability. For this we have considered a slab containing 12 defects in the form of ice sheets.

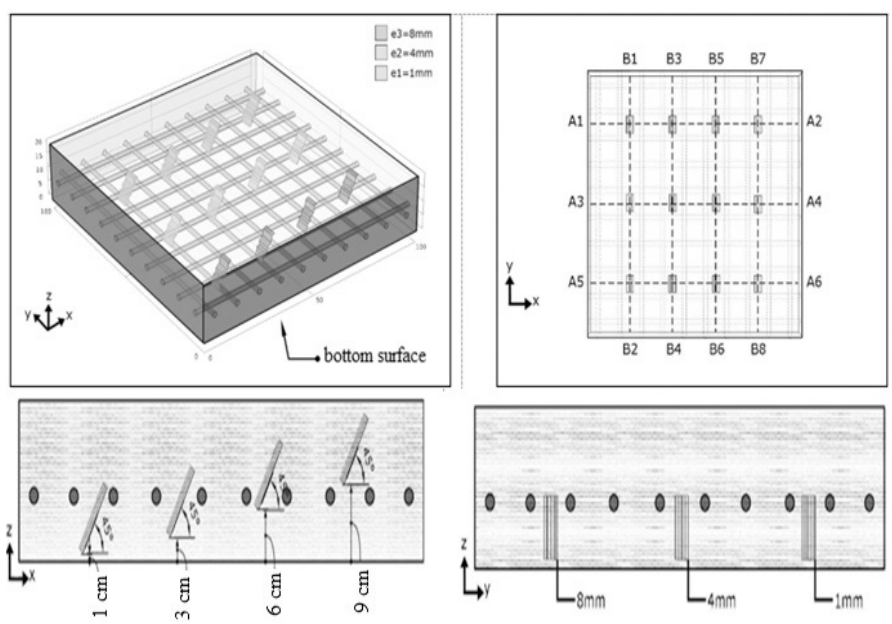

Fig. 6. Location of oblique cracks in the structure.

As shown in Fig. 6, the defects along the lines B1B2, B3B4, B5B6, and B7B8 are, respectively, at the positions p = 1, 3, 6, and 9 cm. And the defects of thicknesses e = 1, 4, and 8 mm are situated, respectively, along the lines A5A6, A3A4, and A1A2.

Effect of crack depth

Fig. 7 shows the distribution of the temperature of the lower surface; one observes three spots of different intensities of such fate that the most intense task is that of thickness e3 = 8 mm, which is at the intersection of the lines A1A2 and B1B2. The direction of inclination is given by the color spectrum of the thermal task at this point, on the thermogram the color changes from blue (colder) to green (less cold), which indicates that the crack tilts to the right. On the curves of evolution of the profile, one realizes that the defect according to each line appears; the maximum difference of temperature ΔT is that which is close to the low surface. Moving away from the surface, the temperature profile begins to become identical to that of a slab without the existence of any defect.

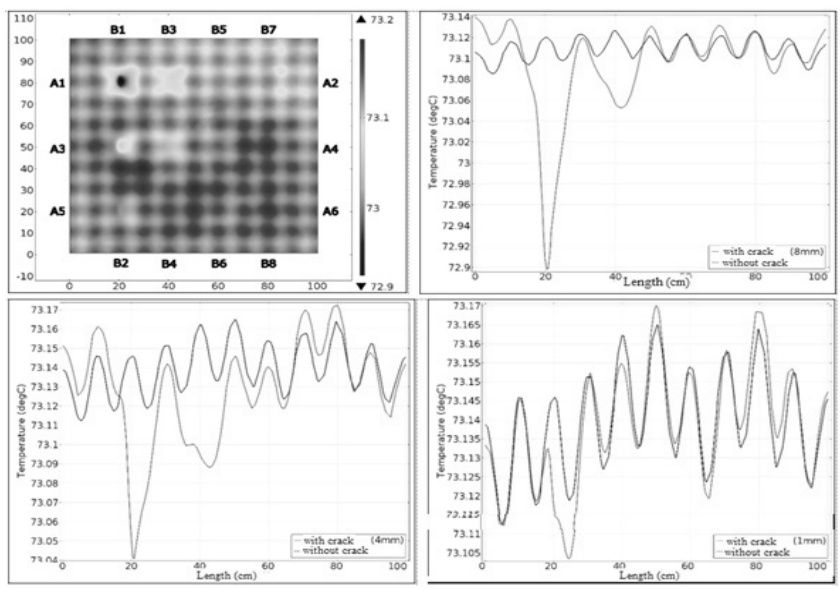

Fig. 7. Temperature distribution along A1A2, A3A4, and A5A6.

Oblique fissures of thickness e1 = 1 mm are not detectable because the temperature profile realized along the line A5A6 is identical to that realized along the same line without existence of the defect. By the same reasoning the cracks found at the intersections of the lines {(A1A2), (B5B6)}, {(A1A2), (B7B8)}, {(A3A4), (B5B6)}, and {(A3A4), (B7B8)} are not detectable.

Effect of crack thickness

From Fig. 8, which represents the evolution of the temperature on the axes B1B2 and B3B4 tangent to the lower face, we notice that there is a thickness influence on the temperature as in the previous cases. The greater the thickness, the greater the difference in temperature, and the defect will be easy to detect.

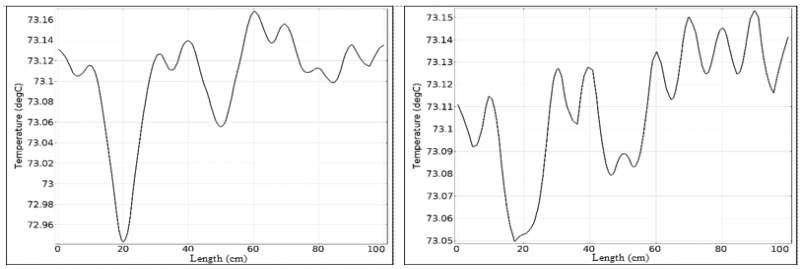

Fig. 8. Temperature distribution along B1B2 (l) and B3B4 (r).

The defects located at the intersection of the lines {(A1A2), (B1B2)}, {(A3A4), (B1B2)}, {(A1A2), (B3B4)}, and {(A3A4), (B3B4)} represent, respectively, a temperature difference of 0.17 °C, 0.06 °C, 0.08 °C, and 0.04°C. These results show that the limit of detectability of oblique fissures is at a depth p = 3 cm and a thickness e = 4 mm.

Effect of tilt angle

In order to study the influence of the position in the detection of oblique defects in a concrete slab, we consider an oblique crack of ice thickness e = 8 mm, placed in the slab to a depth p = 1cm; the crack is inclined at an angle to the low surface, with = 10°, 30°, 50°, and 70°.

The thermograms of Fig. 9 represent the temperature distribution of the lower surface of the slab, and Fig. 10 represents the temperature difference along the AB line for angle values ranging from 10 ° to 70 °.

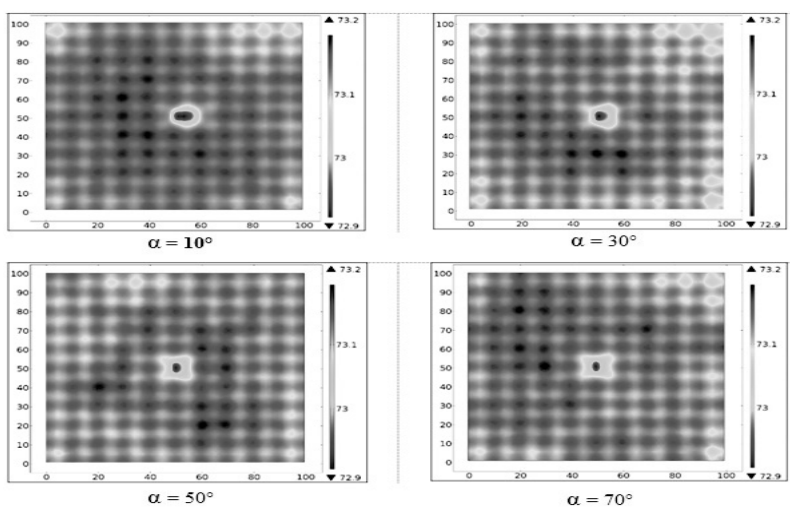

Fig. 9. Thermograms for different inclinations.

The contrast of the blue spots indicating the position of the defects increases as the value of the angle decreases. Indeed, we can notice the same result in Fig. 11. The temperature difference between healthy and defective zones reached 0.25 °C for a defect inclined by an angle = 10°; on the other hand, it only reached 0.16 °C for a defect inclined by an angle = 70°. This shows when one tends from a horizontal defect to a vertical defect, detectability becomes difficult. The contrast is proportional to the temperature drop ΔT between healthy areas and defective areas, but the angle of inclination of the crack affects the contrast of the tasks of the defects in the thermograms.

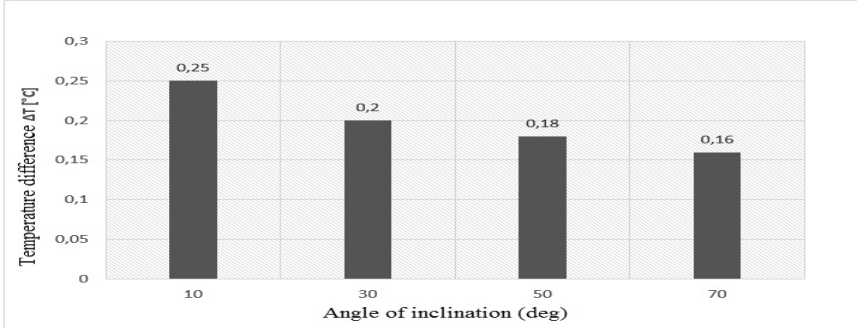

Fig. 10. Histogram of temperature difference along AB.

Effect of bar diameters

We keep the same system of the previous part, in which an oblique crack of thickness e = 8 mm is introduced, placed at a depth p = 1 cm, and inclined at an angle = 45°, with respect to the low surface. The steel bars are, respectively, d = 10 mm, 20 mm, and 32 mm diameter. Fig. 11 shows the simulated thermographic image at the bottom surface of the slab for the three diameters and represents the temperature difference along the AB line in each case.

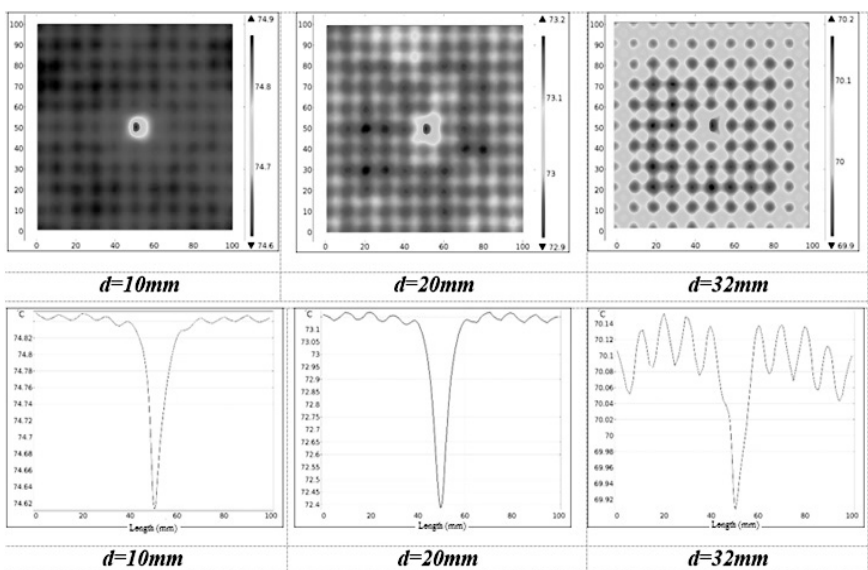

Fig. 11. Temperature distribution for different diameters.

Note that the effect of bar diameter is remarkable on the simulated thermographic image at the entrance surface. In the presence of small diameter bars (d = 10mm), the heat flow propagates better in the structure (due to the decrease of the thermal resistance, which favors the diffusion); hence the rise of the temperature of the latter this elevation is more and more important when the diameter is smaller. This results in a larger temperature difference. Fig. 12 confirms what has been deduced from the preceding figure.

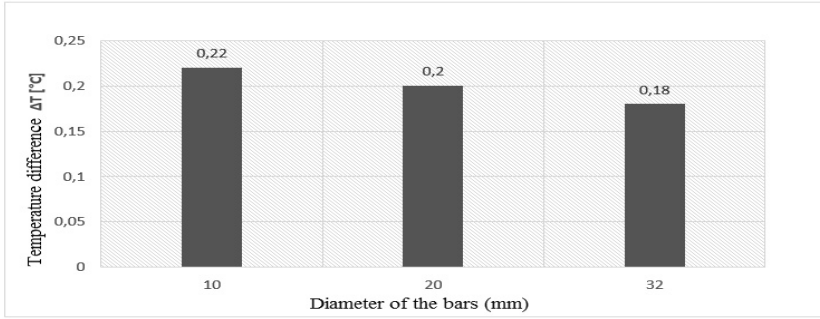

Fig. 12. Histogram of the temperature difference ΔT according to the steel bars.

Effect of thermophysical parameters

In order to illustrate the influence of thermo-physical parameters on the detection of an oblique crack of ice, we consider the slab structure (Fig. 13.a), which contains 3 defects of thickness e = 8 mm, located at a depth p = 1 cm, inclined at an angle = 45 °, with respect to the lower surface (Fig. 13.b).

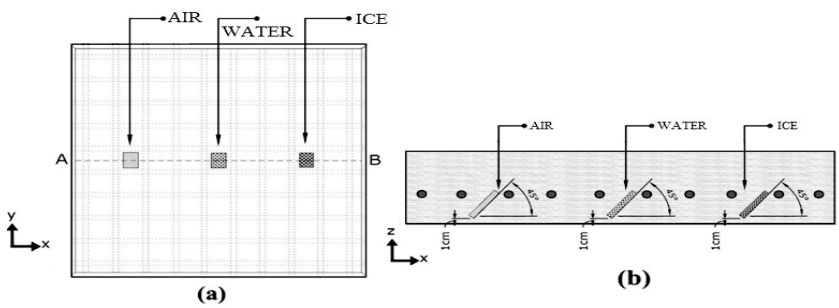

Fig. 13. Structure adopted: (a): upper face; (b): Cross-section according to the plan (xoz).

Fig. 14 represents the simulated thermographic image of the lower surface of the slab with the existence of three vertical cracks of different nature; in the same figure, we represent the temperature profile along the axis AB.

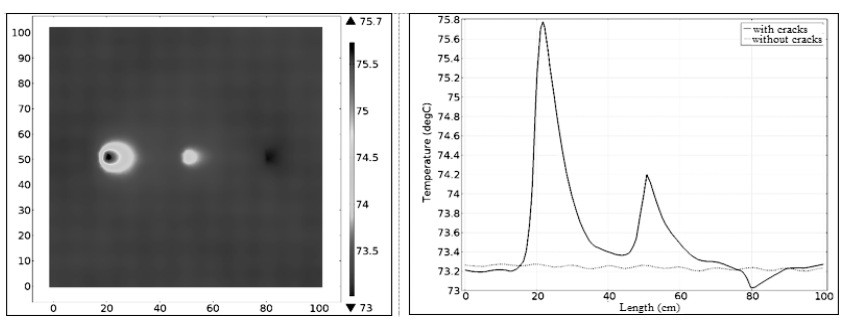

Fig. 14. Thermal image and temperature distribution along the AB.

The figures above show the influence that the nature of the defects can have on the thermographic image; in fact, when the material constituting the crack is a thermal conductor (ice: 1.05 W/m.K), the heat flow is spreading converging towards the defect; hence a decrease in the temperature at the surface occurs. When the material constituting the pipe is a thermal insulator (the air 0.02 W/m.K), the heat flow propagates by avoiding the defect, resulting in a rise of the temperature on the surface directly facing the corresponding pipe.

Temporal study

In this part, we are interested in the temporal study of an oblique crack located in a solid concrete slab. In this part, we consider the same structure of the slab, containing 4 oblique cracks (the cracks detectable in steady state); the cracks along the line A1A2 have a thickness e3 = 8 mm, and a thickness e2 = 4 mm along line A3A4 (Fig.15).

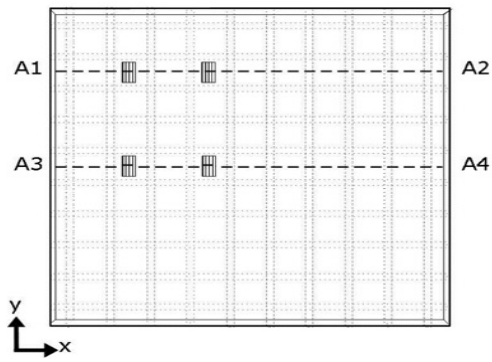

Fig. 15. Face of the adopted structure.

A constant heat flux (Q=500 W/m^2) is applied to the lower surface of the slab for a certain determined period of time in order to cause a temperature difference ΔT sufficiently measurable by the camera between the healthy zones of the slab and the defectives zones. The thermograms in Fig. 16 represent the distribution of the temperature of the bottom surface, and the curves of Fig. 18 represent the evolution of the temperature profiles along the lines A1A2 and A3A4, after a heating period: t1 = 10 min, t2 = 30 min, t3 = 2h, and t4 = 4h.

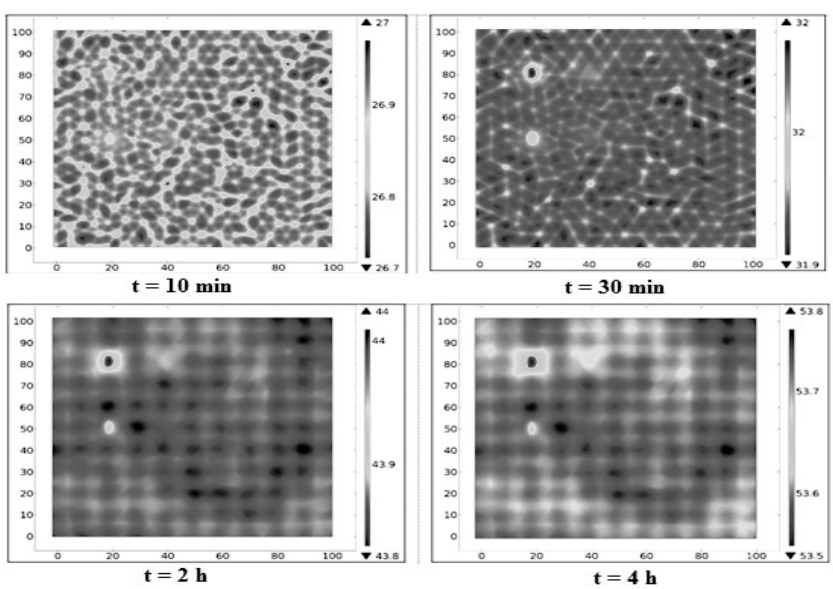

Fig. 16. Thermal images after different durations.

In the thermogram of Fig. 16, we note that 10 min of heating is not sufficient to detect the oblique crack of thickness e3 = 8 mm, located at p = 1 cm, contrary to the cases of horizontal and vertical cracks, which have been detectable easily after the same heating period. Indeed the cracks located at a depth p = 1cm become detectable after 30 min.

such that they have a temperature difference of Ta - Tb = 0.07 °C for the crack thickness e3 = 8 mm, and a temperature difference of Ta - Tb = 0.04 °C for the crack of thickness e2 = 4 mm. In Fig. 17, it is found that the second crack along the A1A2 line begins to appear, and its temperature difference is equal to Ta - Tb = 0.035 °C after 2 hours of heating. By heating the structure a little more at t4 = 4h, on one side, the contrasts of the three fissures analyzed become clearer on the thermograms. The second crack along the line A3A4 is not yet detectable. Moreover, its temperature profile gives no idea about the existence of the latter, which makes the detectability of oblique cracks of thickness e2 = 4 mm and which is at a depth greater than 3 cm very difficult, which is not practicable, especially that infrared cameras can operate up to 4 hours before they are loaded again.

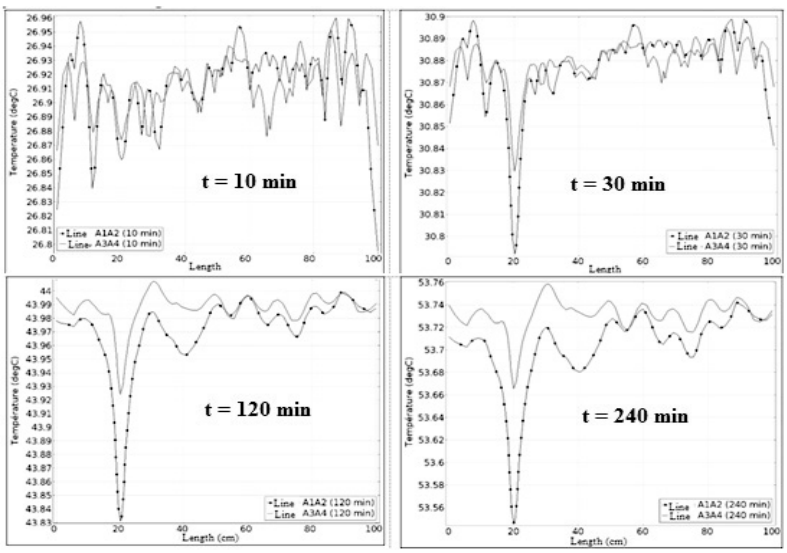

Fig. 17. Temperature distribution on axes A1A2 and A3A4 for different durations.

Study of spherical cracks

Spherical cracks are also one of the flaws that can exist in a reinforced concrete slab. Holes can cause many problems if they are not detected and repaired. In this part, we will use infrared thermography to detect the existence of a spherical crack. In this study, we chose the same structure of dimensions (100 cm x 100 cm x20cm), in which is introduced nine defects of spherical shape are introduced, respectively, having a radius R of 1 cm, 2 cm, and 3 cm, respectively, placed along the lines B1B2, B3B4, and B5B6 (Fig. 18).

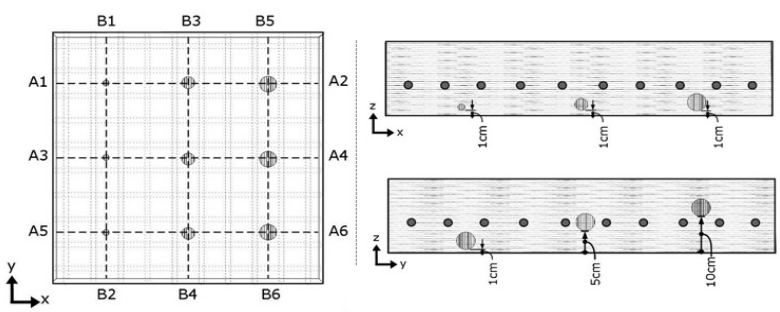

Fig. 18. View of the adopted face.

It is assumed that the initial temperature is T0 = 20 °C. The lower face is subjected to a continuous flow step and extended density (Q = 500 W/m^2). The other faces are isolated.

Effect of geometric parameters

The defects have a spherical shape, the diameter increases if one moves along the X axis, the depth being the same, and on the other hand it varies if one moves along the Y axis, the diameter being constant (Fig. 18).

Effect of depth

In this part, to illustrate the influence of the depth of the defect, we have represented the evolution of the temperature along the axes B1B2, B3B4, and B5B6.

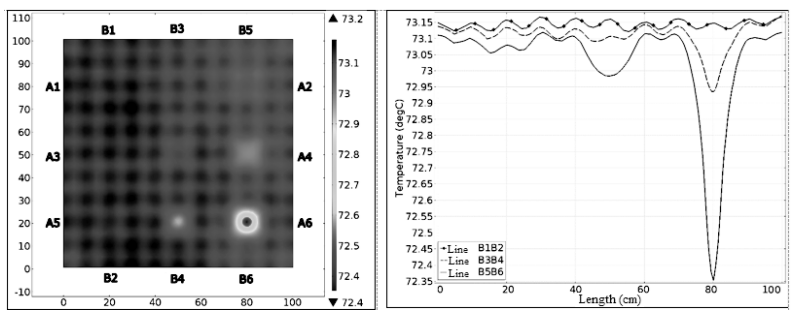

Fig. 19. Thermal image and temperature distribution.

Fig. 19 represents the recorded thermogram of the lower surface and shows the temperature evolution along these axes B1B2, B3B4, and B5B6. The effect of ice hole depth on the surface temperature distribution is remarkable. Indeed, for defects of the same diameter, the closer we get to the surface, the greater the temperature difference associated with the defect becomes important.

Effect of crack thickness

Fig. 20 shows the evolution of the temperature at the surface of the structure, along the axes A1A2, A3A4, and A5A6. The curve shows the influence of the defect thickness on the temperature distribution of the surface; thus, the greater the thickness, the greater the intensity of the contrast, reflecting that the presence of defect is strong and vice versa.

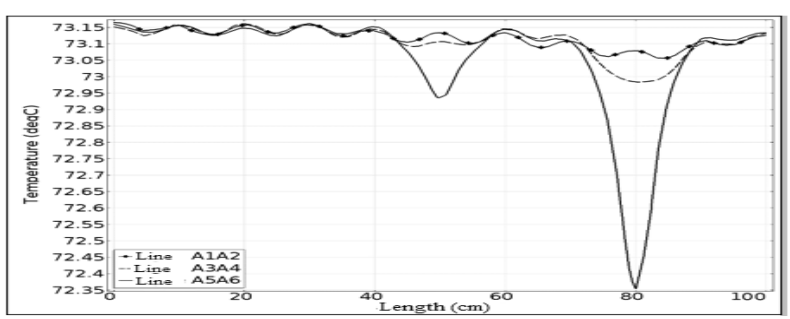

Fig. 20. Temperature evolution along axes A1A2, A3A4, and A5A6.

The defects located at the intersection of the lines {(A5A6), (B3B4)}, {(A3A4), (B5B6)}, and {(A5A6), (B5B6)}, respectively, represent a temperature difference equal to 0.12 ° C, 0.19 ° C, and 0.75 ° C. The other defects inserted are located under the detectability zone, which is ΔT <0.035 ° C (Fig. 21).

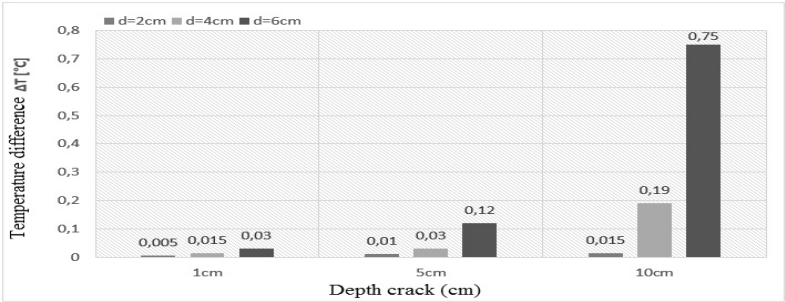

Fig. 21. Histogram of the temperature difference ΔT.

Diameter effect of steel bars

The diameter of the steel reinforcement varies from one slab to another; to study the effect of this parameter on the detection of cracks, we inserted a spherical fissure of radius R = 3 cm in a structure (Fig. 22) of dimensions (100cm x100cm x20cm), to a depth p = 1 cm. The steel bars have, respectively, d = 10 mm, 20 mm, and 32 mm diameter.

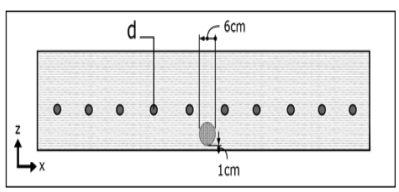

Fig. 22. Cross-section according to plan (xoz).

Fig. 23 shows the simulated thermographic image on the lower surface of the slab and represents the temperature difference along the AB line.

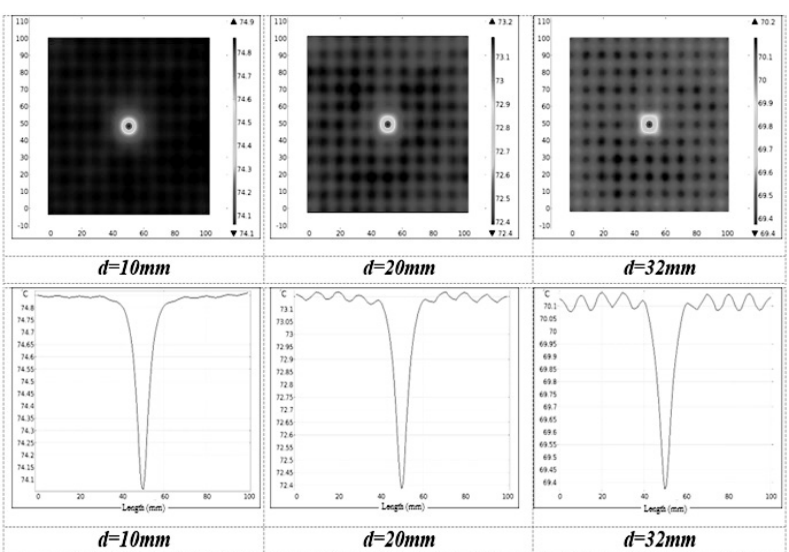

Fig. 23. Temperature evolutions along AB for different diameters.

It is noted that the effect of the diameter of the bars is remarkable on the temperature curves above. In the presence of small diameter bars (d = 10mm), the heat flow propagates better in the structure (due to the decrease of the thermal resistance, which favors diffusion); hence there is a rise in temperature of the latter.

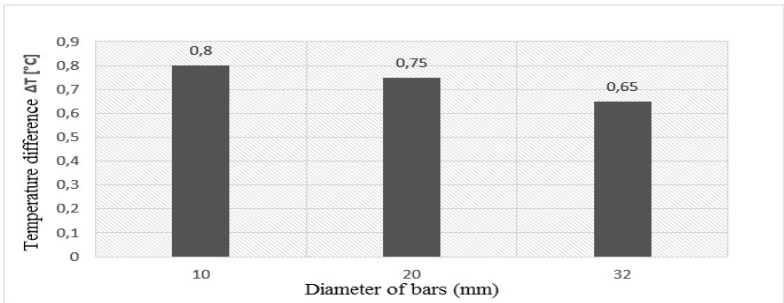

Fig. 24. Histogram of difference temperature for different diameters.

Fig. 24 confirms what was deduced previously. Indeed a crack located at the limit of the detectability zone ($\Delta T = 0.035$ °C) can be undetectable if it is placed in another structure (slab) whose diameter of reinforcement is larger.

Effect of thermophysical parameters

To illustrate the influence of thermophysical default parameters, we consider the same structure of the slab (Fig. 25.a) containing three defects, of different nature, radius R = 3 cm, located at a depth p = 1 cm from the entrance surface (Fig.25.b).

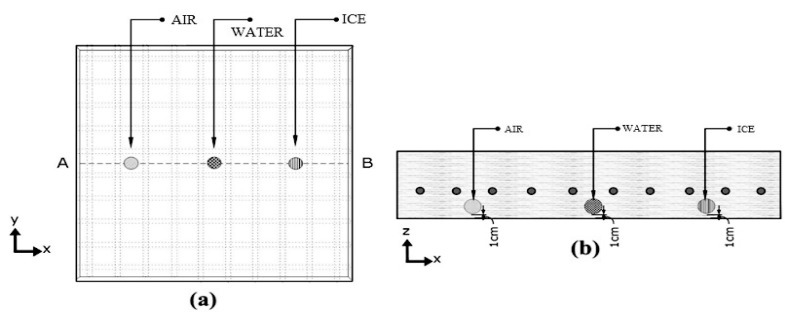

Fig. 25. Description of the structure studied: (a): upper face; (b): Cross-section according to (xoz).

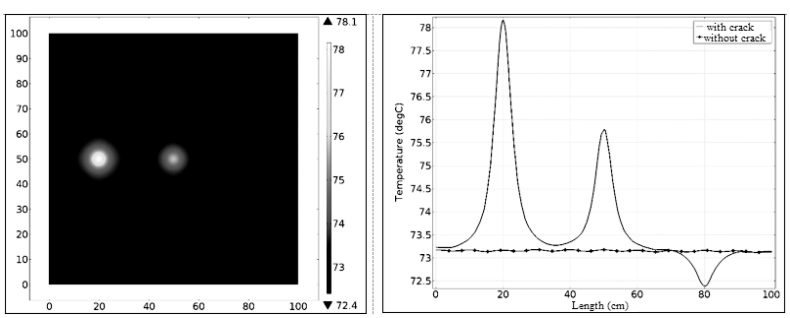

Fig. 26. Thermal image and temperature distribution.

Fig. 26 shows the simulated thermographic image of the inlet surface and shows the temperature profile along the AB line. As in the case of a horizontal, vertical, and oblique crack, the nature of the defect (air, water, and ice) acts differently on the heat flow through the concrete structure. The air and water anomalies accumulate heat, which generates an increase in temperature compared to the neighborhood. In addition, the ice-type anomaly absorbs the heat flow, which causes a drop in temperature in this area compared to its neighborhood. These results can be approached differently by studying the effusivity of these materials, which describes the speed with which a material absorbs calories. The higher the effusivity, the more the material (ice) absorbing energy without noticeably heating up. On the contrary, the weaker it is, the faster the material (steel, air, concrete, and water) heats up. Three values to compare the effusivity of the materials are used, as seen in the Table 2.

Table 2. Thermal effusivity of defects in the slab.

Material	**Effusivity ($J.K^{-1}.cm^{-2}.s^{-1/2}$)**
Air	0.0006
Water	0.16
Ice	0.28

Temporal study

We are interested in the temporal study of a spherical crack located in a reinforced concrete slab. We consider the same structure of the slab, containing 4 spheres of ice, the crack along the line B3B4 has a radius R1 = 2cm, and the cracks of the line B5B6 have a radius R2 = 3 cm (Fig. 27).

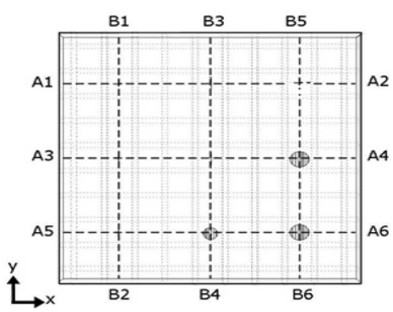

Fig. 27. View of the adopted structure.

The thermograms in Fig. 28 represent the distribution of the temperature of the bottom surface, and the curves in Fig. 29 represent the evolution of temperature profiles along the lines B3B4 and B5B6, after a period of heating: t1 = 7 min, t2 = 20 min, t3 = 1.5 h, and t4 = 4 h.

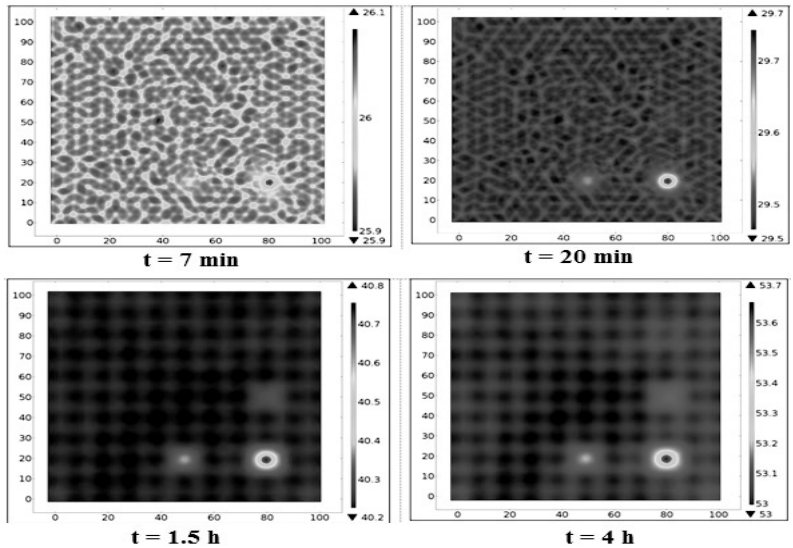

Fig. 28. Thermal images at t = 7 min, 20 min, 1.5 h and t = 4 h.

It is noted on the temperature thermograms above that the effect of the heating period of the structure is strongly related to the detectability of the holes. When the temperature rises, the bars become more visible.

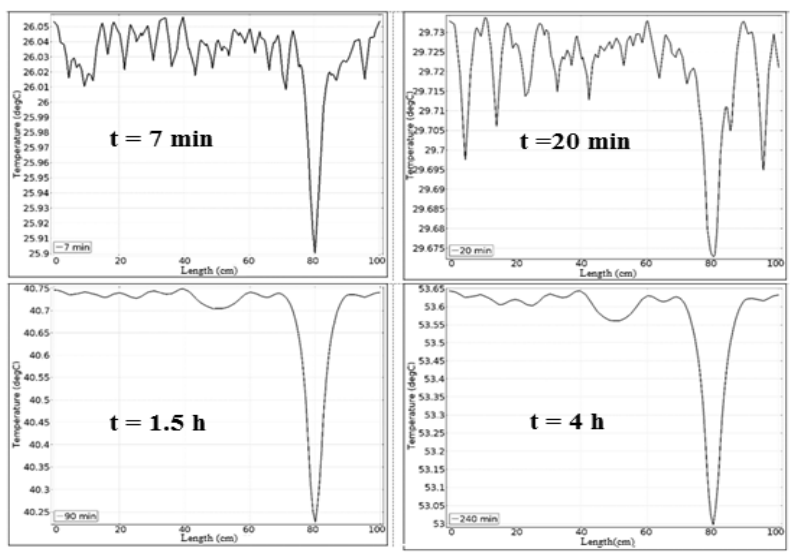

Fig. 29. Temperature distribution along B5B6.

From these figures, we note that the spherical crack located at p = 1cm and radius R = 3 cm is easily detectable after 7 min of heating, with a temperature difference of Ta - Tb = 0.13 °C, which makes this type of crack detectable by the three categories of cameras used in the inspection of civil engineering works. The crack of radius R = 2 cm, placed at the same depth, becomes detectable after 20 min. It is found that the temperature difference at that time $\Delta T = 0.04$ ° C.

In this figure, we notice a temperature peak at the location of the crack located at p = 3 cm along the line B5B6; its temperature difference is equal to $\Delta T = 0.02$ °C after 1.5h of heating. This gap is very difficult to detect and

interpret. By heating the structure a little more at t4 = 4 h, the peak becomes larger, and the temperature difference will equal ΔT = 0.035 °C. This spherical crack becomes better detectable after 4 hours of heating of the structure.

CONCLUSION

In this study, we realized the effect of several parameters on the detectability of cracks in a reinforced concrete slab; these cracks can be horizontal, vertical, oblique, or spherical. In order to know the impact of depth, diameter of the steel bars, and nature of the material of the crack.

The results presented above show:

- Oblique fissures of thickness e = 1 mm, as well as all cracks (whatever e ≤ 8mm) located at a depth not exceeding 3 cm are not detectable
- Under transient conditions only cracks at p = 1 cm are detectable in a reasonable time.

Regarding the spherical fissures:

- The steady-state study showed that holes with radius R = 3 cm are detectable regardless of their position in the slab, and holes with radius greater than or equal to 2 cm, which are located at depths that do not exceed 1cm, are also detectable.
- When working under transient conditions, the detection of a spherical defect will be strongly related to the heating period and the resolution of the equipment used. The higher the resolution of the cameras, the faster the detection is; thus, the more you heat, the more the intensity of the contrast reflecting the presence of defect is clear.
- Some cracks require heating that exceeds four hours, making their detections impractical.

REFERENCES

Al-Kassir , A.R., Fernandez, J., Tinaut, F. & Castro F. 2005. Thermographic study of energetic installations. Applied Thermal Engineering **25**: 183–190.

Belattar, S., Rhazi, J. & Elballouti, A. 2012. Non-destructive testing by infrared thermography of the void and honeycomb type defect in the concrete. International Journal of Microstructure and Materials Properties **7**: 235-253.

Bomberg, M. & Shirtliffe, C. 1988. Influence of moisture and moisture gradients on heat transfer through porous building materials. ASTM STP **660**: 211–233.

Elafi, M., Belatter, S. & Bouferra, R. 2017. Numerical modeling applied to the analysis of defects pipelines and pipes in a concrete wall**.** Journal of Engineering Technology **6**: 449-461.

Grinzato, E., Bison, P. & Marinetti, S. 2002. Monitoring of ancient buildings by the thermal method. Journal of Cultural Heritage **3**: 21–29.

Ibarra, C.C., Galmiche, F., Darabi, A., Pilla, M., Klein, M., Ziadi, A., Vallerand, S., Pelletier, J.F. & Maldague, X.P. 2003. Thermographic nondestructive evaluation: overview of recent progress. Proceeding of Thermosense XXV. Orlando, Florida.

IAEA, 2002. Guidebook on non-destructive testing of concrete structures, IAEA–TCS–17, Vienna.

Kathleen, M. & Massicotte, B. 2004. Fiber reinforced concrete in reinforced bridge deck slab design. Proceeding of the 11th Symposium on the Progress of Quebec Research on Engineering Structures. Montreal, Quebec.

Laure, L. 2006. Concrete cracking analysis and implementation techniques in order to optimize the realization of the works. Report, INSA, Strasbourg, France.

Ljungberg, S.A. 1994. Infrared Techniques in Buildings and Structures: Operation and maintenance. Infrared Methodology and Technology, X.P.V. Maldague, Ed: 211-252.

Maierhofer, C & Roellig, M. 2009. Active thermography for the characterization of surfaces and interfaces of historic masonry

structures. Proceeding of the 7th International Symposium on Non-destructive Testing in Civil Engineering (NDTCE), Nantes, France.

Nguyen, Q.T., Care S., Berthaud Y. & Millard A. 2005. Fissuration du béton soumis à la corrosion. L'objet **8** (2) : 1-15.

Sugiura, R., Noguchi, N. & Ishii, K. 2007. Correction of low-altitude thermal images applied to estimating soil water status. Biosystems Engineering **96**: 301–313.

Usamentiaga, R., Venegas, P., Guerediaga, J., Vega, L., Molleda, J. & Bulnes, G.F. 2014. Infrared Thermography for temperature measurement and non-destructive testing. Sensors **14**: 12305-12348.

Vavilov, V.P. & Nesteruk, D.A. 2004. Detecting water in aviation honeycomb structures: The quantitative approach. Quantitative Infrared Thermography Journal **1**: 173–184

Vollmer, M & M¨ollmann, K.P. 2011. Infrared Thermal Imaging: Fundamentals, Research and Applications. John Wiley & Sons Ed., Weinheim, Germany.

Submitted: 30/12/2017
Revised: 16/03/2018
Accepted: 22/04/2018

طريقة الأشعة تحت الحمراء في الكشف عن العيوب الداخلية لبلاطة من الخرسانة المسلحة

عبد الحميد نوفيد و سقراطي بلعطار
كلية العلوم السملالية، جامعة القاضي عياض، مراكش، 40000، المغرب

الخلاصة

إن تطوير الأساليب العددية للحاسوب قد جعل من المحاكاة الرقمية أداة مهمة جداً في مجال الصناعة وفي مختلف مجالات البحث العلمي .في هذه الدراسة، نحاول أن نقوم بدراسة كاملة قدر الإمكان حول سلوك البلاطة وفقاً للأنماط الشاذة الداخلية التي يمكن أن تلمس هذه الأجزاء من المباني، والتي ترجع من ناحية إلى تأثير التقادم أو الزلازل، ومن ناحية أخرى إلى التغيرات المناخية الدائمة التي تتعرض لها هذه البلاطة أو ببساطة لحوادث غير متوقعة كالإنفجارات. سوف ندرس إمكانية الكشف عن الشقوق الداخلية في بلاطة من الخرسانة المسلحة باستخدام الأشعة تحت الحمراء، حيث أن هذه الأخيرة تدخل في وسائل الاختبار غير المُدمرة للمنشآت المدنية. وبفضل برنامج محاكاة على الكمبيوتر، تمت دراسة هذا النموذج بغرض الحصول على استنتاجات تطبيقية على أرض الواقع. يمكن أن تتمركز هذه التصدعات بشكل أفقي أو عمودي أو مائل أو بأي شكل أخر. علاوة على ذلك، سيتم دراسة سمك البلاط، وعمق التصدع، وطبيعة المواد، وقطر قضبان الصلب ووقت التدفئة في كل من الحالات السابقة الذكر. ووفقاً لهذه الدراسة، فإنه بالإمكان الكشف عن هذه التصدعات عن طريق الأشعة تحت الحمراء إذا توفرت عدد من الشروط فقط، والتي سيتم تفصيلها في هذه الدراسة. كما أنه في بعض الحالات تقف هذه الطريقة عاجزة، مما يستلزم الخروج عن حدود إستعمالها والتي سنتطرق إليها في هذا العمل.